


Cite this: *RSC Adv.*, 2020, 10, 1580

# Sub-millimeter size high mobility single crystal MoSe<sub>2</sub> monolayers synthesized by NaCl-assisted chemical vapor deposition

Juncheng Li,<sup>†a</sup> Wenjie Yan,<sup>†a</sup> Yanhui Lv,<sup>a</sup> Jian Leng,<sup>a</sup> Duan Zhang,<sup>b</sup> Cormac Ó Coileáin,<sup>c</sup> Conor P. Cullen,<sup>c</sup> Tanja Stimpel-Lindner,<sup>d</sup> Georg S. Duesberg,<sup>cd</sup> Jiung Cho,<sup>e</sup> Miri Choi,<sup>f</sup> Byong Sun Chun,<sup>g</sup> Yanfeng Zhao,<sup>a</sup> Chengzhai Lv,<sup>a</sup> Sunil K. Arora<sup>h</sup> and Han-Chun Wu<sup>id</sup>\*<sup>a</sup>

Monolayer MoSe<sub>2</sub> is a transition metal dichalcogenide with a narrow bandgap, high optical absorbance and large spin-splitting energy, giving it great promise for applications in the field of optoelectronics. Producing monolayer MoSe<sub>2</sub> films in a reliable and scalable manner is still a challenging task as conventional chemical vapor deposition (CVD) or exfoliation based techniques are limited due to the small domains/nanosheet sizes obtained. Here, based on NaCl assisted CVD, we demonstrate the simple and stable synthesis of sub-millimeter size single-crystal MoSe<sub>2</sub> monolayers with mobilities ranging from 38 to 8 cm<sup>2</sup> V<sup>-1</sup> s<sup>-1</sup>. The average mobility is 12 cm<sup>2</sup> V<sup>-1</sup> s<sup>-1</sup>. We further determine that the optical responsivity of monolayer MoSe<sub>2</sub> is 42 mA W<sup>-1</sup>, with an external quantum efficiency of 8.22%.

Received 4th November 2019  
Accepted 26th December 2019

DOI: 10.1039/c9ra09103c

rsc.li/rsc-advances

## Introduction

Recently, transition metal dichalcogenides (TMDCs) have received considerable attention owing to their narrow direct bandgaps and great potential for use in electronics and optoelectronics, catalysts, capacitors, and novel heterostructures.<sup>1–3</sup> MoSe<sub>2</sub> is a TMDC with many unique properties and is a route to explore their applications.<sup>4–6</sup> Phototransistors based on MoSe<sub>2</sub> have been shown to display a very quick response time (<25 ms) at room temperature under ambient conditions.<sup>7,8</sup> The edge sites of MoSe<sub>2</sub> nanofilms and nanosheets have been found to be electrochemically active for H<sub>2</sub>.<sup>9,10</sup> It has also been shown that mesoporous MoSe<sub>2</sub> based anodes are an alternative for lithium

ion batteries, with a reversible and stable storage capacity of 630 mA h g<sup>-1</sup>.<sup>11,12</sup> Heterostructures incorporating MoSe<sub>2</sub> have been reported to exhibit a strong photocurrent response and photovoltaic effect with high quantum efficiency.<sup>13</sup> MoSe<sub>2</sub> monolayers are the most promising candidate, among these materials, for applications in the field of optoelectronics due to the narrow direct bandgap (1.55 eV), high optical absorbance and large spin-splitting energy.<sup>2,4,11,14</sup>

There are many different ways to produce MoSe<sub>2</sub>.<sup>4,14–16</sup> However, producing monolayer MoSe<sub>2</sub> films in a reliable and scalable manner is still a challenging task. The most common approaches are mechanical exfoliation and CVD.<sup>17–20</sup> Although simple and convenient, exfoliation as a method usually suffers from some drawbacks. The product is usually multilayered, meaning it has an indirect bandgap and relatively weak optoelectronic performance.<sup>21</sup> The lateral dimensions of exfoliated monolayer TMDCs are as small as a few tens of nm to several micrometers, which poses difficulties for its laboratory investigation and use.<sup>2</sup> Furthermore, contamination in the exfoliation processes is unavoidable. Comparatively, CVD can produce larger, purer and monolayer materials.<sup>20,22</sup> Reports on the CVD growth of MoSe<sub>2</sub> suggest that it is extremely difficult to synthesize large area continuous monolayer films with solid-phase precursors because of the low chemical reactivity of Se.<sup>23–25</sup> The CVD synthesis of MoSe<sub>2</sub> results in triangular-shaped discontinuous domains of either single-layer MoSe<sub>2</sub> or mixtures of single- and few-layer MoSe<sub>2</sub>.<sup>20,26,27</sup> In addition, CVD is known to suffer from a lack of steady and durable output, which prevents its more widespread use for the production of monolayer MoSe<sub>2</sub> films.<sup>28</sup> To overcome some of the challenges

<sup>a</sup>School of Physics, Beijing Institute of Technology, Beijing 100081, P. R. China. E-mail: wuhc@bit.edu.cn

<sup>b</sup>Elementary Educational College, Beijing Key Laboratory for Nano-Photonics and Nano-Structure, Capital Normal University, Beijing 100048, P. R. China

<sup>c</sup>Centre for Research on Adaptive Nanostructures and Nanodevices (CRANN), Advanced Materials and Bioengineering Research (AMBER), School Chemistry, Trinity College Dublin, Ireland

<sup>d</sup>Institute of Physics, EIT 2, Faculty of Electrical Engineering and Information Technology, Universität der Bundeswehr München, Germany

<sup>e</sup>Western Seoul Center, Korea Basic Science Institute, Seoul 03579, Republic of Korea

<sup>f</sup>Chuncheon Center, Korea Basic Science Institute, Chuncheon 24341, Republic of Korea

<sup>g</sup>Division of Industrial Metrology, Korea Research Institute of Standards and Science, Daejeon 305-340, Republic of Korea

<sup>h</sup>Centre for Nanoscience and Nanotechnology, Panjab University, Chandigarh-160014, India

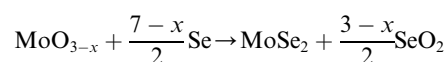
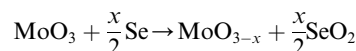
<sup>†</sup> These authors contributed equally to this work.



associated with the CVD growth of TMDs using solid-phase precursors, recently NaCl has been used to assist the CVD growth of MoS<sub>2</sub> and WS<sub>2</sub> monolayers.<sup>29–31</sup> It was found that the addition of NaCl led to an enhancement of the growth rate, reduced growth temperature and more continuous film production, due to formation of intermediate Na-containing species that reduce the energy of the reaction. The size of MoS<sub>2</sub> and WS<sub>2</sub> monolayers grown by this method were found to reach 300 μm (ref. 29) and 500 μm (ref. 31) respectively. However, to the best of our knowledge, there is little data on electrical and photoelectrical properties of TMDCs monolayers prepared by the NaCl assisted CVD method. In this work, we extended the above methodology to MoSe<sub>2</sub> monolayer synthesis. Using NaCl assisted CVD, we have developed a simple and stable CVD method to synthesize large-scale, single crystal and monolayered MoSe<sub>2</sub>, whose size can be up to 250 μm. We also study the electrical and optoelectronic properties of the MoS<sub>2</sub> monolayers in a four fingered back-gated field-effect transistor (FET) and find that they are n-type with an average mobility of 12 cm<sup>2</sup> V<sup>−1</sup> s<sup>−1</sup> and responsivity of 42 mA W<sup>−1</sup>.

## Results and discussion

Fig. 1(a) shows a schematic of the CVD growth system. MoO<sub>3</sub> powder and Se particles were used as precursors. NaCl was used to assist the reaction. A SiO<sub>2</sub> (300 nm)/Si substrate was put on the boat containing MoO<sub>3</sub> powder with its polished surface facing downward in the quartz boat to receive sufficient mass flux of metal precursor. In conventional CVD, the process of MoSe<sub>2</sub> monolayer growth is a step-by-step nucleation.<sup>29</sup> The two main reactions involved in MoSe<sub>2</sub> growth are:



The first reaction occurs mainly during the temperature ramp-up period while the second reaction, which is called an epitaxial process, takes place in the steady temperature period.

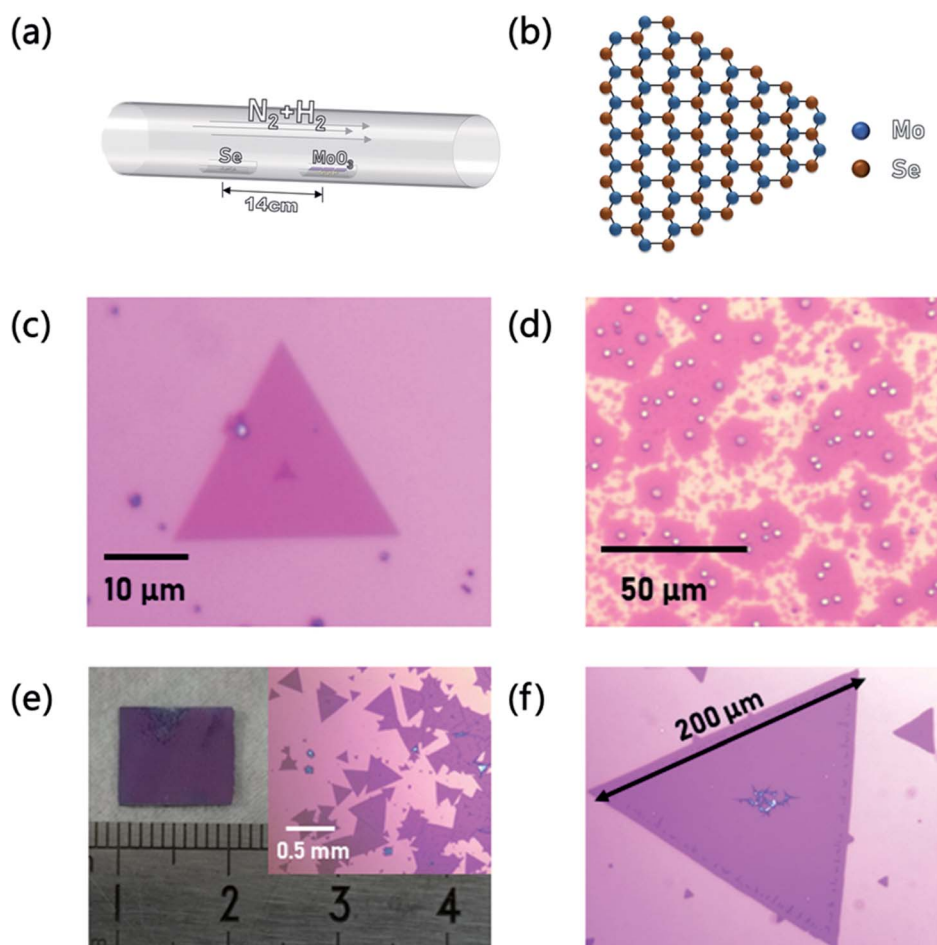


**Fig. 1** (a) Schematic of CVD growth system. (b) Atomistic model of monolayer MoSe<sub>2</sub>. (c) Image of MoSe<sub>2</sub> grown by standard conditions without NaCl, using 15.6 mg MoO<sub>3</sub> as the precursor. (d) Image of MoSe<sub>2</sub> grown with the same conditions without NaCl, using 16.6 mg MoO<sub>3</sub> as the precursor. (e) Typical appearance of prepared MoSe<sub>2</sub> on the substrate. The dark purple layers, contrast with the pink substrate, are visible monolayers of MoSe<sub>2</sub>. (f) MoSe<sub>2</sub> triangle of typical size of grown with the assistance of NaCl.



As a result, the core-like dots at the center of many of the MoSe<sub>2</sub> monolayers are essentially suboxide compounds, MoO<sub>3-x</sub>Se<sub>y</sub>, rather than the MoSe<sub>2</sub> at the core. Moreover, the anisotropic growth of MoSe<sub>2</sub> proceeds by different modes when there is a different ratio between Mo and Se, resulting in two kinds of edges, Mo-edges and Se-edges (Fig. 1(b)).<sup>31</sup> When the ratio between Mo and Se atoms is close to 1 : 2, the shape of the MoSe<sub>2</sub> flakes looks like a regular hexagon. If Mo atoms are greater in abundance, the Mo-edge grows relatively faster.<sup>15,27,32</sup> Following standard practice, when we use a relatively small quantity of MoO<sub>3</sub> powder, the process yields low density small monolayer MoSe<sub>2</sub> triangles. When more MoO<sub>3</sub> is used, there is densely distributed isotropic MoSe<sub>2</sub> (Fig. 1(c and d)). Clearly, the change of ratio between Mo and Se in the reaction, created by the great abundance of MoO<sub>3</sub>, results in the change in observed morphology.

To overcome above issues, NaCl has been used to assist the CVD growth. In the NaCl assisted CVD method, NaCl has a two-fold effect on the growth process as below:<sup>33</sup>



First, it can accelerate the growth of MoSe<sub>2</sub>, with the formation of MoO<sub>2</sub>Cl<sub>2</sub>, which provides an opportunity for gas-phase reactions among MoO<sub>2</sub>Cl<sub>2</sub>, Se and H<sub>2</sub>. Secondly, it can increase the mass flux of the metal precursors by decreasing the melting point of MoO<sub>3</sub>, producing higher

nucleation density. To avoid over-nucleation, a small quantity of MoO<sub>3</sub> powder is used. Fig. 1(e) shows a typical optical image of a monolayer MoSe<sub>2</sub> film grown by NaCl assisted CVD. It shows both large-scale and dense monolayer MoSe<sub>2</sub> coverage. The typical lateral size of MoSe<sub>2</sub> grown with the NaCl assisted CVD is more than 200 μm (Fig. 1(f)), and some can reach up to 500 μm.

Fig. 2(a) shows an atomic force microscopy (AFM) image of as-prepared MoSe<sub>2</sub>. Clear contrast between the SiO<sub>2</sub>/Si substrate and MoSe<sub>2</sub> indicates that the thickness is ~0.82 nm. In addition to verifying the uniformity of the layers, we also identify the phase of the complete monolayer as MoSe<sub>2</sub> using the Raman spectroscopy (Fig. 2(b)).<sup>28</sup> The Raman spectra consists of two main peaks at 240 cm<sup>-1</sup> and 520 cm<sup>-1</sup>. The peak at 520 cm<sup>-1</sup> is the characteristic Raman peak of the Si, while the one at 240 cm<sup>-1</sup> indicates the dominance of the A<sub>1g</sub> mode, the out of plane vibration, of MoSe<sub>2</sub>.<sup>34,35</sup> We also find Raman peaks at 169 cm<sup>-1</sup>, 289 cm<sup>-1</sup> and 361 cm<sup>-1</sup>, corresponding the E<sub>1g</sub>, E<sub>2g</sub> and A<sub>2g</sub>, modes of MoSe<sub>2</sub> respectively. We used transmission electron microscopy (TEM) to verify the monolayer nature and crystal structure of the MoSe<sub>2</sub>. The measured width of the lattice fringes is 0.27 nm which is in agreement with reports on the distance between the adjacent atoms.<sup>5</sup> Selected-area-electron-diffraction (SAED) images of MoSe<sub>2</sub> (inset of Fig. 2(c)) exhibit one set of six-fold symmetry diffraction spots, confirming its highly crystalline monolayer nature. From energy-dispersive X-ray spectroscopy (EDS) mapping of a MoSe<sub>2</sub> sample exposed to atmosphere, the ratio between Mo and Se atoms is determined to be close to 1 : 2, displaying the stability of MoSe<sub>2</sub>. The stability of MoSe<sub>2</sub> and its adhesion to the Si/SiO<sub>2</sub> substrate was

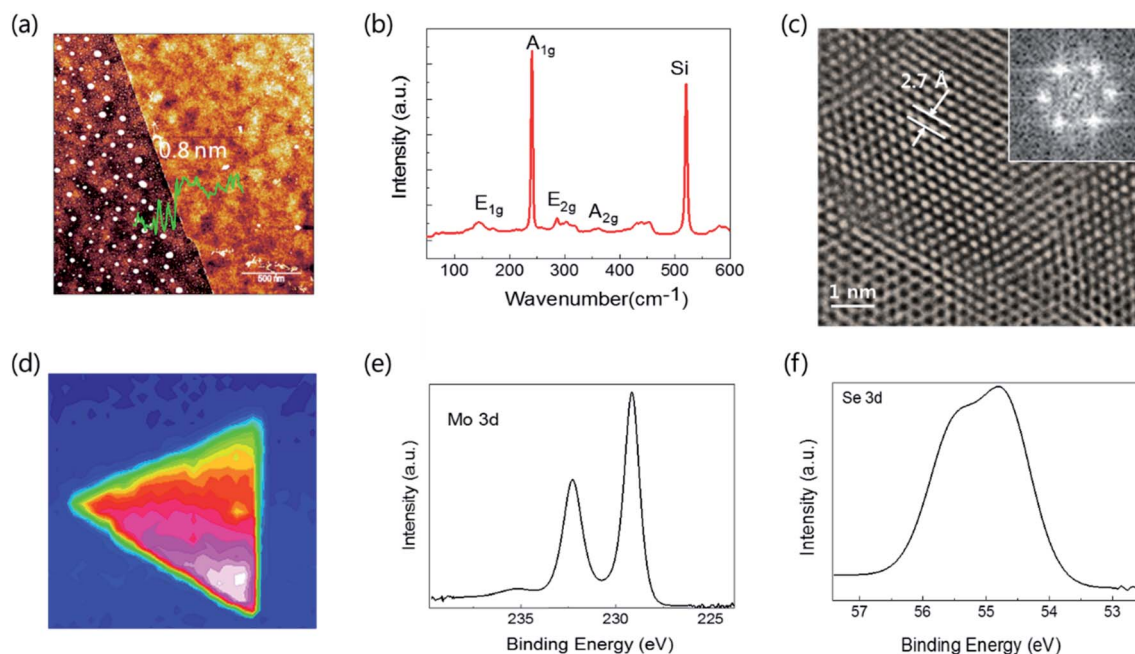


Fig. 2 (a) AFM height map of MoSe<sub>2</sub> sample on growth substrate. Also shown in the figure is the height profile near the edge of a MoSe<sub>2</sub> domain. (b) Raman spectra of MoSe<sub>2</sub> sample, showing the major observed peaks. (c) High resolution TEM image of MoSe<sub>2</sub> sample with its selected area diffraction pattern shown in the inset. (d) Raman mapping of MoSe<sub>2</sub> sample. (e and f) XPS spectra recorded for Mo 3d and Se 3d edges at room temperature for monolayer MoSe<sub>2</sub> sample.



further checked by soaking it in water, ethanol and acetone. Fig. 2(e) shows X-ray photoelectron spectroscopy (XPS) core level spectra of the Mo-3d and Se-3d core-levels of the as grown MoSe<sub>2</sub> monolayer films measured at 300 K. From the data we can determine that there is only one major state for the Mo and two states for Se atoms, the binding energy for the Mo-Se Mo 3d<sub>5/2</sub> state is 229.1 eV. While the corresponding values for the Se 3d<sub>5/2</sub> 55.5 eV. Both elements showed minor components at higher binding energies attributed to surface oxygen absorption as the sample was exposed to ambient conditions for an extended period.<sup>36</sup>

In order to study the electrical and optoelectronic properties of MoSe<sub>2</sub>, we fabricated four-finger back-gated field-effect transistors. The output and transfer characteristics of a MoSe<sub>2</sub> FET is shown in Fig. 3. The output and transfer characteristics are evidence of the n-type nature of the MoSe<sub>2</sub>, which is in-line with the previous studies.<sup>16,31,37,38</sup> Fig. 3(a and b) shows the  $I_d$ - $V_d$  characteristic under gate voltages ranging from -16 V to +4 V. The curve shows the obvious semiconducting nature of MoSe<sub>2</sub>, whose resistance decreases as the bias voltage increases. In contrast with conventional FETs, there is no apparent saturation in the drain current the FETs fabricated from MoSe<sub>2</sub>. The switching voltage without a gate voltage is about 12 V, while the positive/negative gate voltage can decrease/increase the switching voltage. As expected, gate voltage can modulate the conductivity of the FET. Fig. 3(c) exhibits the  $I_d$ - $V_g$  characteristic measured under different bias voltage. The FET is depleted from free carriers when  $V_g$  is lower than 0 V. The switch ratio,  $I_{on}/I_{off}$ , under +4 V of bias voltage, can reach  $10^5$ .<sup>39-42</sup> The transfer characteristic offers the opportunity to compute the mobility of the FET. Using the

formula  $\mu = \frac{dI_d L}{dV_g W C_{SiO_2} V_d}$ , we find that the mobility  $\mu$  is  $20.1 \text{ cm}^2 \text{ V}^{-1} \text{ s}^{-1}$ . In this formula,  $L$  and  $W$  are the length and width of the conduction channel, respectively, and  $C_{SiO_2} = \epsilon_0 \epsilon_r / d$  is capacitance per unit area estimated for the gate dielectric, with  $\epsilon_0$  being the free-space permittivity,  $\epsilon_r$ , the relative permittivity for SiO<sub>2</sub>, being 3.9, and  $d$ , the thickness of the SiO<sub>2</sub>, being 300 nm. More than 20 devices were fabricated and characterized. It was found that the mobility ranged from 38 to  $8 \text{ cm}^2 \text{ V}^{-1} \text{ s}^{-1}$  (Fig. 3(d)), with an average  $12 \text{ cm}^2 \text{ V}^{-1} \text{ s}^{-1}$ . The highest mobility found for our samples is very close to the reported value ( $50 \text{ cm}^2 \text{ V}^{-1} \text{ s}^{-1}$ ) for mechanically exfoliated ultra-thin MoSe<sub>2</sub>.<sup>43</sup> The reduced mobility can be attributed to imperfections in the monolayers, such as Se vacancies, which might be improved by reducing nuclei density, controlling the mass flux or growth rate, *etc.*<sup>31</sup>

In order to realize the potential of monolayer MoSe<sub>2</sub> for applications in solar cells, photosensitive sensor and other devices,<sup>18,44</sup> it is also necessary to investigate its optoelectronic properties. We measured the optoelectronic responsivity in ambient conditions with different voltages and light sources of different wavelengths. Fig. 4(a) exhibits the quick response time of the FET under the  $200\text{--}500 \text{ mW cm}^{-2}$  power laser with a 635 nm wavelength. The bias voltage is 10 V and the gate voltage is 10 V. Under such conditions, the photocurrent ranges between a few to hundreds of nanoamperes. When the laser power is increased sufficiently, there is saturation of the photo-enhancement of the drain current as can be seen in Fig. 4(b). We also investigate the time response of the gated FET under pulsed 400  $\text{mW cm}^{-2}$  illumination (Fig. 4(c)). It is apparent that a positive gate voltage not only elevates the drain current in both

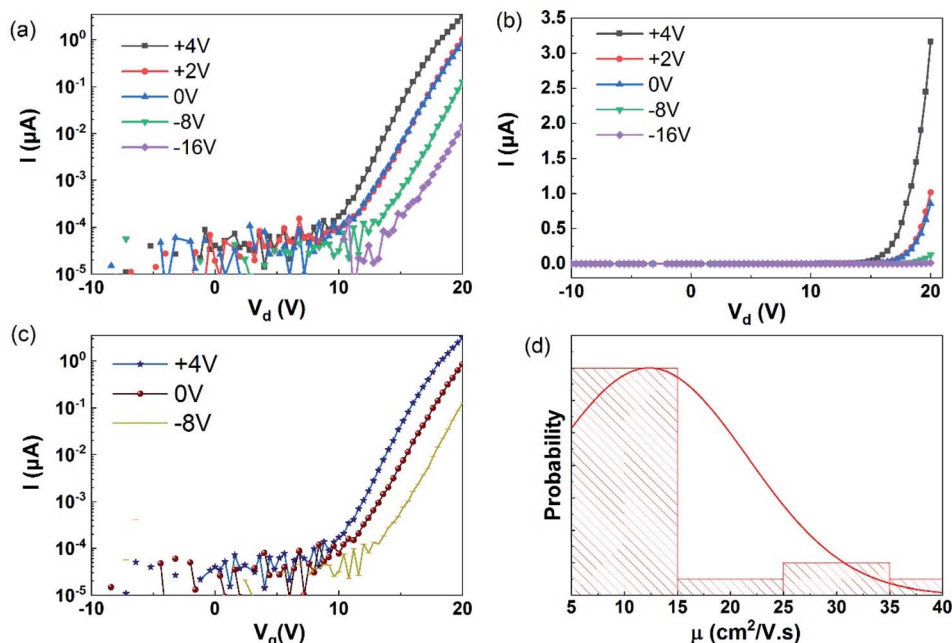


Fig. 3 (a) The  $I$ - $V_d$  curves of the MoSe<sub>2</sub> FET under various gate voltages plotted on a log scale and (b) on a linear scale. (c) Transfer characteristic curve of the FET under various bias voltages. (d) Distribution of the mobility of all devices measured.



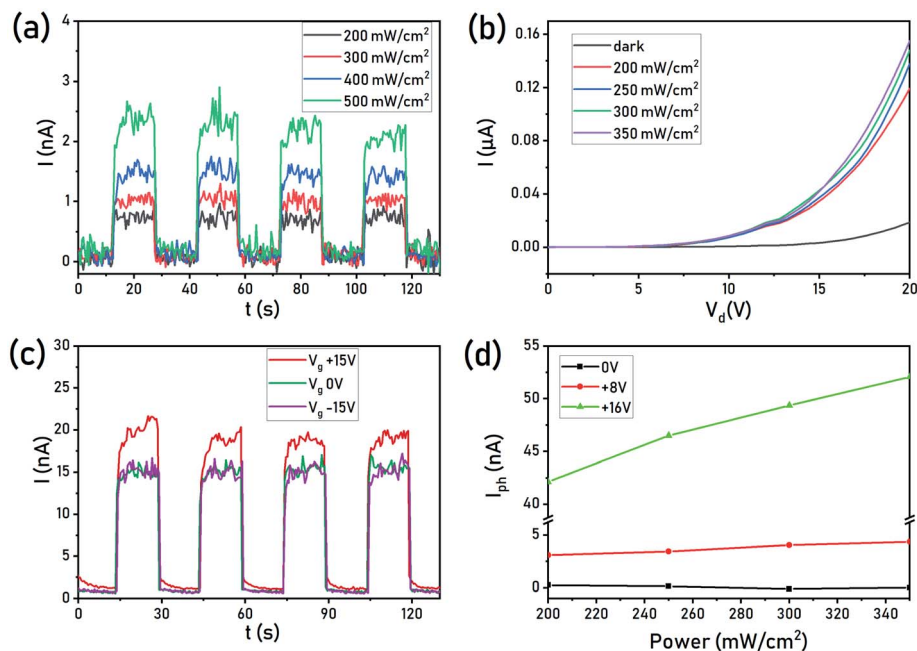


Fig. 4 (a)  $I$ - $t$  characteristic plots for FET for a variety of power intensities of a 635 nm laser. (b) The output characteristic of the FET under different power intensities of 635 nm laser. (c)  $I$ - $t$  characteristic curve of the FET under different gate voltages for the 635 nm laser. (d) The  $I_{\text{photo}}$ -power curve of the FET under different bias voltages.

Table 1 List of electrical and optoelectronic properties from other studies

| Type       | Method                      | Mobility ( $\text{cm}^2 \text{V}^{-1} \text{s}^{-1}$ ) | Responsivity ( $\text{mA W}^{-1}$ ) | Size ( $\mu\text{m}$ ) | Reference |
|------------|-----------------------------|--|-------------------------------------|------------------------|-----------|
| Monolayer  | CVD                         | 23   | —                                   | ~5                     | 8         |
| Film       | CVD                         | 0.02   | —                                   | ~0.2 (grain size)      | 26        |
| Multilayer | CVD                         | 121  | —                                   | Several hundred        | 37        |
| Monolayer  | CVD                         | 50   | —                                   | 135                    | 34        |
| Multilayer | Micromechanical exfoliation | 50   | —                                   | 1–3                    | 16        |
| Monolayer  | CVD                         | —  | 13                                  | >50                    | 21        |
| Ultra-thin | Mechanical exfoliation      | 50.5   | —                                   | <44 $\mu\text{m}$      | 43        |
| Multilayer | Mechanical exfoliation      | 19.7   | 97 100                              | ~30                    | 45        |
| Multilayer | Atomic layer deposition     | —  | 11.7                                | Several hundred        | 46        |
| Multilayer | Mechanical exfoliation      | 30–35  | —                                   | ~10                    | 47        |
| Monolayer  | CVD                         | 42   | —                                   | Several hundred        | 48        |
| Multilayer | CVD                         | 10   | 93 700                              | 3–4                    | 49        |
| Multilayer | Mechanical exfoliation      | 50.6   | 519 200                             | ~10                    | 50        |
| Few layer  | Mechanical exfoliation      | 5.1  | 238 000                             | ~25                    | 51        |
| Monolayer  | CVD                         | 38   | 42                                  | Several hundred        | Our work  |

dark and lit condition, but also increases the photo current, while a negative gate voltage has no such effect. We show the power dependence of the  $I_{\text{photo}}$  in Fig. 4(d) derived from the Fig. 4(b), which intuitively presents the modulation of the bias voltage and the laser power. When the bias voltage climbs into a certain range, the photo current can be modulated by the power intensity, which is shown in Fig. 4(d). We determine the responsivity of the FET to be  $42 \text{ mA W}^{-1}$ , and the external quantum efficiency (EQE) of the device is 8.22%. Table 1 summarizes the electrical and optoelectronic properties of  $\text{MoSe}_2$  from other studies from literature. Clearly, it is rather difficult to synthesize both high-mobility and large-scale

monolayer  $\text{MoSe}_2$ . Using NaCl assisted CVD method, it is relatively easy to synthesize large monolayer  $\text{MoSe}_2$  with sound electrical and optoelectronic properties.

## Conclusion

In conclusion, we have found an effective and convenient method to synthesize large-scale monolayer  $\text{MoSe}_2$  and investigated the optoelectronic properties of derived FETs. When as-prepared  $\text{MoSe}_2$  was used to fabricate FETs, it had a mobility up to  $38 \text{ cm}^2 \text{V}^{-1} \text{s}^{-1}$  and a responsivity of  $42 \text{ mA W}^{-1}$ , which is promising for its practical application.



## Materials and methods

### Sample preparation and characterization

For the reaction, 0.5 g of selenium granules and 5–7 mg of a mixture of MoO<sub>3</sub> powder and 1 mg of sodium chloride powder, were prepared as precursors. We used a quartz boat containing selenium granules and another boat with the mixed NaCl and MoO<sub>3</sub> powder to obtain layered MoSe<sub>2</sub> by the selenization of MoO<sub>3</sub>. Before heating the furnace, 100 standard cubic meter per minute (sccm) of the mixture of H<sub>2</sub>/N<sub>2</sub> (10 : 90) carrier gas was used to purge the tube for 20 minutes. The furnace was heated to 750 °C in 15 minutes with the rate of 50 °C per minute, and a reaction dwell time of 15 minutes was used, after which the furnace was allowed to cool naturally. During the heating and reaction process, the flow rate of the carrier gas was kept at 50 sccm, giving a H<sub>2</sub> flow of 5 sccm. The pressure inside the tube was maintained at 30 Torr. Atomic force microscopy (Bruker Multi-mode 8, in peak force tapping mode), Raman spectroscopy (Bruker Senterra confocal spectrometer with an excitation wavelength of 532 nm), Transmission electronic microscopy (JEOL JEM-2100F at 200 kV with a probe size under 0.5 nm), and XPS (micro-XPS, PHI Versa Probe III) were used to characterize the MoSe<sub>2</sub> samples, identifying its single-layer and high-quality nature. In Raman spectroscopy measurements, the wavelength of the laser used was 532 nm.

### Device fabrication and measurement

The MoSe<sub>2</sub> films were transferred onto new 300 nm SiO<sub>2</sub>/Si substrates using a PMMA assisted transfer method. Ultraviolet lithography was then used to pattern the electrodes. We deposited Ti–Au electrodes with 15 nm of Ti and 55 nm of Au using electron beam evaporation. The channel lengths and widths were 4 μm and 50 μm respectively. For electrical measurements, the devices was placed in a darkness, except for when required, and at room-temperature. In all experiments the source was grounded.

## Author contributions

H. C. W. conceived the study. J. C. L., and J. L. grew the sample. W. J. Y., Y. H. L. and D. Z. performed the Raman measurements. C. C. conducted the AFM characterization. C. P. C., T. S., and G. S. D. performed the XPS characterization. J. C., M. C., and B. S. C. carried out the TEM measurements. Y. F. Z., C. Z. L. and S. K. A. helped with device fabrication and data analysis. H. C. W. and J. C. L. wrote the manuscript. All authors discussed the results and commented on the manuscript.

## Conflicts of interest

There is no conflicts to declare.

## Acknowledgements

This work was supported by the National Key Research and Development Program under grant No. 2017YFA0303800 and

2017YFE0301404, the National Natural Science Foundation of China (No. 61874010, 11804237), and by the Science and Technology Innovation Program for Creative Talents in Beijing Institute of Technology (No. 2017CX01006). G. S. D. acknowledges the support of SFI under Contract No. PI\_15/IA/3131.

## References

- 1 L. Kou, T. Frauenheim and C. Chen, Nanoscale Multilayer Transition-Metal Dichalcogenide Heterostructures: Band Gap Modulation by Interfacial Strain and Spontaneous Polarization, *J. Phys. Chem. Lett.*, 2013, **4**(10), 1730–1736, DOI: 10.1021/jz400668d.
- 2 M. Pumera, Z. Sofer and A. Ambrosi, Layered transition metal dichalcogenides for electrochemical energy generation and storage, *J. Mater. Chem. A*, 2014, **2**(24), 8981–8987.
- 3 M. Bernardi, M. Palummo and J. C. Grossman, Extraordinary sunlight absorption and one nanometer thick photovoltaics using two-dimensional monolayer materials, *Nano Lett.*, 2013, **13**(8), 3664–3670.
- 4 S. Tongay, J. Zhou, C. Ataca, K. Lo, T. S. Matthews, J. Li, J. C. Grossman and J. Wu, Thermally driven crossover from indirect toward direct bandgap in 2D semiconductors: MoSe<sub>2</sub> versus MoS<sub>2</sub>, *Nano Lett.*, 2012, **12**(11), 5576–5580.
- 5 Y. Zhang, T. R. Chang, B. Zhou, Y. T. Cui, H. Yan, Z. Liu, F. Schmitt, J. Lee, R. Moore, Y. Chen, H. Lin, H. T. Jeng, S. K. Mo, Z. Hussain, A. Bansil and Z. X. Shen, Direct observation of the transition from indirect to direct bandgap in atomically thin epitaxial MoSe<sub>2</sub>, *Nat. Nanotechnol.*, 2014, **9**(2), 111–115.
- 6 K. F. Mak and J. Shan, Photonics and optoelectronics of 2D semiconductor transition metal dichalcogenides, *Nat. Photonics*, 2016, **10**(4), 216–226.
- 7 A. Kumar and P. K. Ahluwalia, Electronic structure of transition metal dichalcogenides monolayers 1H-MX<sub>2</sub> (M = Mo, W; X = S, Se, Te) from ab-initio theory: new direct band gap semiconductors, *Eur. Phys. J. B*, 2012, **85**(6), 186.
- 8 Y. H. Chang, W. Zhang, Y. Zhu, Y. Han, J. Pu, J. K. Chang, W. T. Hsu, J. K. Huang, C. L. Hsu, M. H. Chiu, T. Takenobu, H. Li, C. I. Wu, W. H. Chang, A. T. Wee and L. J. Li, Monolayer MoSe<sub>2</sub> grown by chemical vapor deposition for fast photodetection, *ACS Nano*, 2014, **8**(8), 8582–8590.
- 9 C. Xu, S. Peng, C. Tan, H. Ang, H. Tan, H. Zhang and Q. Yan, Ultrathin S-doped MoSe<sub>2</sub> nanosheets for efficient hydrogen evolution, *J. Mater. Chem. A*, 2014, **2**(16), 5597–5601.
- 10 C. Tsai, K. Chan, F. Abild-Pedersen and J. K. Nørskov, Active edge sites in MoSe<sub>2</sub> and WSe<sub>2</sub> catalysts for the hydrogen evolution reaction: a density functional study, *Phys. Chem. Chem. Phys.*, 2014, **16**(26), 13156–13164.
- 11 Y. Shi, C. Hua, B. Li, X. Fang, C. Yao, Y. Zhang, Y.-S. Hu, Z. Wang, L. Chen, D. Zhao and G. D. Stucky, Highly Ordered Mesoporous Crystalline MoSe<sub>2</sub> Material with Efficient Visible-Light-Driven Photocatalytic Activity and Enhanced Lithium Storage Performance, *Adv. Funct. Mater.*, 2013, **23**(14), 1832–1838.



- 12 B. Shin, Y. Zhu, N. A. Bojarczuk, S. J. Chey and S. Guha, Control of an interfacial MoSe<sub>2</sub> layer in Cu<sub>2</sub>ZnSnSe<sub>4</sub> thin film solar cells: 8.9% power conversion efficiency with a TiN diffusion barrier, *Appl. Phys. Lett.*, 2012, **101**(5), 053903.
- 13 Y. Gong, S. Lei, G. Ye, B. Li, Y. He, K. Keyshar, X. Zhang, Q. Wang, J. Lou, Z. Liu, R. Vajtai, W. Zhou and P. M. Ajayan, Two-Step Growth of Two-Dimensional WSe<sub>2</sub>/MoSe<sub>2</sub> Heterostructures, *Nano Lett.*, 2015, **15**(9), 6135–6141.
- 14 J. C. Shaw, H. Zhou, Y. Chen, N. O. Weiss, Y. Liu, Y. Huang and X. Duan, Chemical vapor deposition growth of monolayer MoSe<sub>2</sub> nanosheets, *Nano Res.*, 2014, **7**(4), 511–517.
- 15 S. Larentis, B. Fallahazad and E. Tutuc, Field-effect transistors and intrinsic mobility in ultra-thin MoSe<sub>2</sub> layers, *Appl. Phys. Lett.*, 2012, **101**(22), 223104.
- 16 J. N. Coleman, M. Lotya, A. O'Neill, S. D. Bergin, P. J. King, U. Khan, K. Young, A. Gaucher, S. De, R. J. Smith, I. V. Shvets, S. K. Arora, G. Stanton, H. Y. Kim, K. Lee, G. T. Kim, G. S. Duesberg, T. Hallam, J. J. Boland, J. J. Wang, J. F. Donegan, J. C. Grunlan, G. Moriarty, A. Shmeliov, R. J. Nicholls, J. M. Perkins, E. M. Grievson, K. Theuwissen, D. W. McComb, P. D. Nellist and V. Nicolosi, Two-dimensional nanosheets produced by liquid exfoliation of layered materials, *Science*, 2011, **331**(6017), 568–571.
- 17 D. Jariwala, V. K. Sangwan, L. J. Lauhon, T. J. Marks and M. C. Hersam, Emerging device applications for semiconducting two-dimensional transition metal dichalcogenides, *ACS Nano*, 2014, **8**(2), 1102–1120.
- 18 J. Shen, Y. He, J. Wu, C. Gao, K. Keyshar, X. Zhang, Y. Yang, M. Ye, R. Vajtai, J. Lou and P. M. Ajayan, Liquid Phase Exfoliation of Two-Dimensional Materials by Directly Probing and Matching Surface Tension Components, *Nano Lett.*, 2015, **15**(8), 5449–5454.
- 19 R. Ge, X. Wu, M. Kim, J. Shi, S. Sonde, L. Tao, Y. Zhang, J. C. Lee and D. Akinwande, Atomrstor: Nonvolatile Resistance Switching in Atomic Sheets of Transition Metal Dichalcogenides, *Nano Lett.*, 2018, **18**(1), 434–441.
- 20 J. Xia, X. Huang, L. Z. Liu, M. Wang, L. Wang, B. Huang, D. D. Zhu, J. J. Li, C. Z. Gu and X. M. Meng, CVD synthesis of large-area, highly crystalline MoSe<sub>2</sub> atomic layers on diverse substrates and application to photodetectors, *Nanoscale*, 2014, **6**(15), 8949–8955.
- 21 Q. H. Wang, K. Kalantar-Zadeh, A. Kis, J. N. Coleman and M. S. Strano, Electronics and optoelectronics of two-dimensional transition metal dichalcogenides, *Nat. Nanotechnol.*, 2012, **7**(11), 699–712.
- 22 Y. Shi, H. Li and L. J. Li, Recent advances in controlled synthesis of two-dimensional transition metal dichalcogenides via vapour deposition techniques, *Chem. Soc. Rev.*, 2015, **44**(9), 2744–2756.
- 23 A. S. Pawbake, M. S. Pawar, S. R. Jadkar and D. J. Late, Large area chemical vapor deposition of monolayer transition metal dichalcogenides and their temperature dependent Raman spectroscopy studies, *Nanoscale*, 2016, **8**(5), 3008–3018.
- 24 M. I. B. Utama, X. Lu, Y. W. Yuan and Q. H. Xiong, Detrimental influence of catalyst seeding on the device properties of CVD-grown 2D layered materials: a case study on MoSe<sub>2</sub>, *Appl. Phys. Lett.*, 2014, **105**(25), 253102.
- 25 D. Hu, G. Xu, L. Xing, X. Yan, J. Wang, J. Zheng, Z. Lu, P. Wang, X. Pan and L. Jiao, Two-Dimensional Semiconductors Grown by Chemical Vapor Transport, *Angew. Chem., Int. Ed.*, 2017, **56**(13), 3611–3615.
- 26 X. Lu, M. I. Utama, J. Lin, X. Gong, J. Zhang, Y. Zhao, S. T. Pantelides, J. Wang, Z. Dong, Z. Liu, W. Zhou and Q. Xiong, Large-area synthesis of monolayer and few-layer MoSe<sub>2</sub> films on SiO<sub>2</sub> substrates, *Nano Lett.*, 2014, **14**(5), 2419–2425.
- 27 X. Song, Z. Guo, Q. Zhang, P. Zhou, W. Bao and D. W. Zhang, Progress of Large-Scale Synthesis and Electronic Device Application of Two-Dimensional Transition Metal Dichalcogenides, *Small*, 2017, **13**(35), 1700098.
- 28 H. Li, Y. Li, A. Aljarb, Y. Shi and L. J. Li, Epitaxial Growth of Two-Dimensional Layered Transition-Metal Dichalcogenides: Growth Mechanism, Controllability, and Scalability, *Chem. Rev.*, 2018, **118**(13), 6134–6150.
- 29 Y. P. Shi, P. F. Yang, S. L. Jiang, Z. P. Zhang, Y. H. Huan, C. Y. Xie, M. Hong, J. P. Shi and Y. F. Zhang, Na-assisted fast growth of large single-crystal MoS<sub>2</sub> on sapphire, *Nanotechnology*, 2019, **30**(3), 034002.
- 30 Z. Wang, Y. Xie, H. Wang, R. Wu, T. Nan, Y. Zhan, J. Sun, T. Jiang, Y. Zhao, Y. Lei, M. Yang, W. Wang, Q. Zhu, X. Ma and Y. Hao, NaCl-assisted one-step growth of MoS<sub>2</sub>-WS<sub>2</sub> in-plane heterostructures, *Nanotechnology*, 2017, **28**(32), 325602.
- 31 J. Zhou, J. Lin, X. Huang, Y. Zhou, Y. Chen, J. Xia, H. Wang, Y. Xie, H. Yu, J. Lei, D. Wu, F. Liu, Q. Fu, Q. Zeng, C. H. Hsu, C. Yang, L. Lu, T. Yu, Z. Shen, H. Lin, B. I. Yakobson, Q. Liu, K. Suenaga, G. Liu and Z. Liu, A library of atomically thin metal chalcogenides, *Nature*, 2018, **556**(7701), 355–359.
- 32 J. Chen, B. Liu, Y. Liu, W. Tang, C. T. Nai, L. Li, J. Zheng, L. Gao, Y. Zheng, H. S. Shin, H. Y. Jeong and K. P. Loh, Chemical Vapor Deposition of Large-Sized Hexagonal WSe<sub>2</sub> Crystals on Dielectric Substrates, *Adv. Mater.*, 2015, **27**(42), 6722–6727.
- 33 X. Duan, C. Wang, J. C. Shaw, R. Cheng, Y. Chen, H. Li, X. Wu, Y. Tang, Q. Zhang, A. Pan, J. Jiang, R. Yu, Y. Huang and X. Duan, Lateral epitaxial growth of two-dimensional layered semiconductor heterojunctions, *Nat. Nanotechnol.*, 2014, **9**(12), 1024–1030.
- 34 X. Wang, Y. Gong, G. Shi, W. L. Chow, K. Keyshar, G. Ye, R. Vajtai, J. Lou, Z. Liu, E. Ringe, B. K. Tay and P. M. Ajayan, Chemical vapor deposition growth of crystalline monolayer MoSe<sub>2</sub>, *ACS Nano*, 2014, **8**(5), 5125–5131.
- 35 H. Terrones, E. Del Corro, S. Feng, J. M. Poumirol, D. Rhodes, D. Smirnov, N. R. Pradhan, Z. Lin, M. A. Nguyen, A. L. Elias, T. E. Mallouk, L. Balicas, M. A. Pimenta and M. Terrones, New first order Raman-active modes in few layered transition metal dichalcogenides, *Sci. Rep.*, 2014, **4**, 4215.



- 36 J. Lu, A. Carvalho, X. K. Chan, H. Liu, B. Liu, E. S. Tok, K. P. Loh, A. Castro Neto and C. H. Sow, Atomic healing of defects in transition metal dichalcogenides, *Nano Lett.*, 2015, **15**(5), 3524–3532.
- 37 J. S. Rhyee, J. Kwon, P. Dak, J. H. Kim, S. M. Kim, J. Park, Y. K. Hong, W. G. Song, I. Omkaram, M. A. Alam and S. Kim, High-Mobility Transistors Based on Large-Area and Highly Crystalline CVD-Grown MoSe<sub>2</sub> Films on Insulating Substrates, *Adv. Mater.*, 2016, **28**(12), 2316–2321.
- 38 G. W. Shim, K. Yoo, S. B. Seo, J. Shin, D. Y. Jung, I. S. Kang, C. W. Ahn, B. J. Cho and S. Y. Choi, Large-area single-layer MoSe<sub>2</sub> and its van der Waals heterostructures, *ACS Nano*, 2014, **8**(7), 6655–6662.
- 39 T. Chen, G. Hao, G. Wang, B. Li, L. Kou, H. Yang, X. Zheng and J. Zhong, Controlled growth of atomically thin MoSe<sub>2</sub> films and nanoribbons by chemical vapor deposition, *2D Mater.*, 2019, **6**(2), 025002.
- 40 Q. Feng, M. Zhu, Y. Zhao, H. Liu, M. Li, J. Zheng, H. Xu and Y. Jiang, Chemical vapor deposition growth of sub-centimeter single crystal WSe<sub>2</sub> monolayer by NaCl-assistant, *Nanotechnology*, 2019, **30**(3), 034001.
- 41 V. K. Sangwan, D. Jariwala, I. S. Kim, K.-S. Chen, T. J. Marks, L. J. Lauhon and M. C. Hersam, Gate-tunable memristive phenomena mediated by grain boundaries in single-layer MoS<sub>2</sub>, *Nat. Nanotechnol.*, 2015, **10**(5), 403.
- 42 H. Fang, S. Chuang, T. C. Chang, K. Takei, T. Takahashi and A. Javey, High-performance single layered WSe<sub>2</sub> p-FETs with chemically doped contacts, *Nano Lett.*, 2012, **12**(7), 3788–3792.
- 43 S. Larentis, B. Fallahazad and E. Tutuc, Field-effect transistors and intrinsic mobility in ultra-thin MoSe<sub>2</sub> layers, *Appl. Phys. Lett.*, 2012, **101**, 223104.
- 44 M. L. Tsai, S. H. Su, J. K. Chang, D. S. Tsai, C. H. Chen, C. I. Wu, L. J. Li, L. J. Chen and J. H. He, Monolayer MoS<sub>2</sub> heterojunction solar cells, *ACS Nano*, 2014, **8**(8), 8317–8322.
- 45 A. Abderrahmane, P. J. Ko, T. V. Thu, S. Ishizawa, T. Takamura and A. Sandhu, High photosensitivity few-layered MoSe<sub>2</sub> back-gated field-effect phototransistors, *Nanotechnology*, 2014, **25**(36), 365202.
- 46 T. J. Dai, X. D. Fan, Y. X. Ren, S. Hou, Y. Y. Zhang, L. X. Qian, Y. R. Li and X. Z. Liu, Layer-controlled synthesis of wafer-scale MoSe<sub>2</sub> nanosheets for photodetector arrays, *J. Mater. Sci.*, 2018, **53**(11), 8436–8444.
- 47 S. R. Das, J. Kwon, A. Prakash, C. J. Delker, S. Das and D. B. Janes, Low-frequency noise in MoSe<sub>2</sub> field effect transistors, *Appl. Phys. Lett.*, 2015, **106**(8), 083507.
- 48 Y. Gong, G. Ye, S. Lei, G. Shi, Y. He, J. Lin, X. Zhang, R. Vajtai, S. T. Pantelides, W. Zhou, B. Li and P. M. Ajayan, Synthesis of Millimeter-Scale Transition Metal Dichalcogenides Single Crystals, *Adv. Funct. Mater.*, 2016, **26**(12), 2009–2015.
- 49 C. Jung, S. M. Kim, H. Moon, G. Han, J. Kwon, Y. K. Hong, I. Omkaram, Y. Yoon, S. Kim and J. Park, Highly Crystalline CVD-grown Multilayer MoSe<sub>2</sub> Thin Film Transistor for Fast Photodetector, *Sci. Rep.*, 2015, **5**, 15313.
- 50 H. Lee, J. Ahn, S. Im, J. Kim and W. Choi, High-Responsivity Multilayer MoSe<sub>2</sub> Phototransistors with Fast Response Time, *Sci. Rep.*, 2018, **8**, 11545.
- 51 P. J. Ko, A. Abderrahmane, N. H. Kim and A. Sandhu, High-performance near-infrared photodetector based on nano-layered MoSe<sub>2</sub>, *Semicond. Sci. Technol.*, 2017, **32**(6), 065015.

